Penerbit Akademia Baru

Journal of Advanced Research in Numerical Heat Transfer

Journal homepage:
http://www.akademiabaru.com/submit/index.php/arnht/index
ISSN: 2735-0142

Effect of Surface Roughness and Induced Magnetic Field on Electro-Osmosis Peristaltic Flow of Eyring Powell Nanofluid in a Tapered Asymmetric Channel

Asha S Kotnurkar[1,*], Namrata Kallolikar[1]

[1] Department of Mathematics, Karnatak University, Dharwad-58003, Karantaka, India

ABSTRACT

In the present analysis, the electro-osmosis peristaltic flow of Eyring Powell nanofluid in a tapered asymmetric channel is considered. The effects of induced magnetic field and boundary sinusoidal roughness are also retained. Using suitable non-dimensional terms the governing equations are transformed into a system of nonlinear partial differential equations. To study the flow, the analytic formulation of flow velocity, pressure gradient, temperature, concentration, volume fraction, stream function and magnetic force function has been analyzed. From the study, it is observed that pressure rise enlarges and velocity diminishes with an increase in the roughness parameter, however, the surface of trapped bolus becomes rough by increasing the roughness parameter and the volume of trapped bolus decreases by increasing the volume flow rate, and Hartmann number. The outcome of the present study helps to investigate the roughness of biological organs such as blood flow in coronary arteries and roughness exists on all other surfaces up to some extent. It can also be used to identify diseases within biological tissues.

Keywords:
Peristaltic flow; Eyring-Powell nanofluid;
induced magnetic field; double diffusion;
electro-osmosis

Received: 24 May 2022 **Revised: 23 July 2022** **Accepted: 19 August 2022** **Published: 7 November 2022**

1. Introduction

Researchers have been studying peristaltic transport over the past few decades because of its applicability in industry and physiology. Peristalsis is a longitudinal wave of relaxation or extension passing through a channel or cylinder. Peristalsis' pumping mechanism is implicated in the physiology of diverse biological organs, and the mechanism has also been used in industrial applications. Latham [1] came up with the term "peristalsis" in 1966, and Shapiro *et al.,* [2] and Jaffrin *et al.,* [3] continued to explore peristaltic flow in various geometries. Many empirical investigations on peristalsis motion have been reported for fluids flow in different channels. Some of them are Asha *et al.,* [4-5] studied peristaltic flow of nanofluid in the presence of gold nanoparticles of a Jeffrey fluid. Further, Aamir *et al.,* [6] focused on the peristalsis of nanofluid in a deformable channel with double diffusion.

*Corresponding author.
E-mail address: ashask@kud.ac.in (Asha S Kotnurkar)

Understanding the peristaltic flow under the influence of roughness of surface on during movement of biological fluids is very beneficial to understand various problems related to blood flow in coronary arteries. Investigation of the effects of endothelium roughness on blood and roughness of coronary arteries has been studied by Burton *et al.,* [7] and Park *et al.,* [8]. The influence of surface roughness on flow has piqued the interest of chemical engineers who want to learn more about the consequences of roughness of walls, formed due to chemical erosion during chemical transportation and some of the studies are [9-10]. Several research studies in this field have used mini channels, micro channels, and sand tubes with the organised roughness of a sinusoidal form given in the references [11-13]. Some recent studies on surface roughness in peristalsis are [14-15]. The term "taper" refers to a decrease in thickness from one point to the other. Asymmetric peristalsis fluid flow in a two-dimensional infinite non-uniform channel was used to simulate the tapered asymmetric channel. It's usually caused by myometrial contractions causing intra-uterine fluid flow. Eytan *et al*., [16] examined peristalsis in a tapered channel having application to embryo transport within the uterine cavity. Some other studies on tapered asymmetric channels are [17-19].

Mechanism of electro-osmosis is described as a process in which applied electric potential causes mobility in an ionised solution (electrolyte) contained in a channel when a solid surface comes into contact with electrolyte solution in electroosmosis flow, a charge is induced on it. The electric potential on the surface attracts opposite ions to the surface in this process, resulting in the development of an electron double layer (EDL). When an external electric field is given to an ionic solution, the Coulomb force is produced, which causes fluid motion. This phenomenon is employed in bio microfluidic systems to regulate the flow of fluid through minuscule channels. Micro electromechanical systems (MEMS), micro peristaltic pumps, lab-on-chip are examples of bio microfluidics devices that use electroosmosis and EDL principles. Capillary electrophoresis is a key component in the development of DNA analysis techniques. As a result, electro-osmotically moving fluid influenced by peristaltic pumping may be employed in DNA analysis, which can then be used in DNA sequencing, DNA length determination, and genetic disease detection. Some recent studies on electro-osmosis are [20-23].

In recent years, bio-magnetic fluid dynamics has been a major research area. It is due to numerous applications in biotechnology and medicinal science, such as the development of magnetic devices for cell separation, drug delivery to the focused organs using magnetic particles as drug carriers. Recently, the influence of magnetic field on the peristalsis of Newtonian and non-Newtonian fluids has been studied [24–26]. The salient features of an induced magnetic field have been ignored in all of these researches. Vishnyakov *et al.,* [27] first to investigate the influence of an induced magnetic field on peristalsis. They looked at a conductive Newtonian fluid's peristaltic MHD flow. They solved the problem using the asymptotic narrowband approach, and only produced velocity profiles in certain channel cross-sections. Recent studies on induced magnetic field on peristaltic flow are [28-29]. Convection that is caused by two distinct density gradients with differing diffusion rates is known as double-diffusive convection. Study of double-diffusion has got a lot of attention from investigators because of the numerous applications it has in industries and engineering, such as oceanography, solid-state physics, and astrophysics. Because of the many benefits of double-diffusive convection, it was investigated in peristaltic pumping using a nanofluid flow model. Few investigations on peristalsis were examined by [30-31].

Non-Newtonian fluids have recently gained a lot of attention due to their applications in medical science and industry. In both physiology and industry, viscoelastic fluids play an important role. Eyring-Powell is a type of non-Newtonian fluid model that includes elasticity as well as viscosity and it is useful for obtaining accurate viscous nanofluid findings at low and high shear rates. Because of their numerous uses in applied engineering, medical sciences and industry, such as the extraction

of crude oil from petroleum oil products, the manufacturing of syrup medications, and the creation of plastic materials. The Eyring-Powell model, which is developed from the idea of rate processes, can characterise the shear of a non-Newtonian flow. In some cases, this model may be used to characterise the viscosity of polymer solutions and viscoelastic suspensions over a broad range of shear rates. Recent studies on the Eyring-Powell nanofluids are [32-33].

From the above investigations shows that no effort has been carried out to study the effect of surface roughness and induced magnetic field with dependency double diffusion convection on electro-osmosis peristaltic flow. The dimensionless equations are resolved using the Homotopy perturbation Sumudu transformation method (HPSTM) [34-38]. The numerical results of pertained physical parameter on fluid flow are analysed in detailed through graphs.

2. Mathematical analysis

Consider the propagation of peristalsis of bi-dimensional tapered asymmetric channel of width d and sinusoidal-shaped roughness shown in Figure 1.

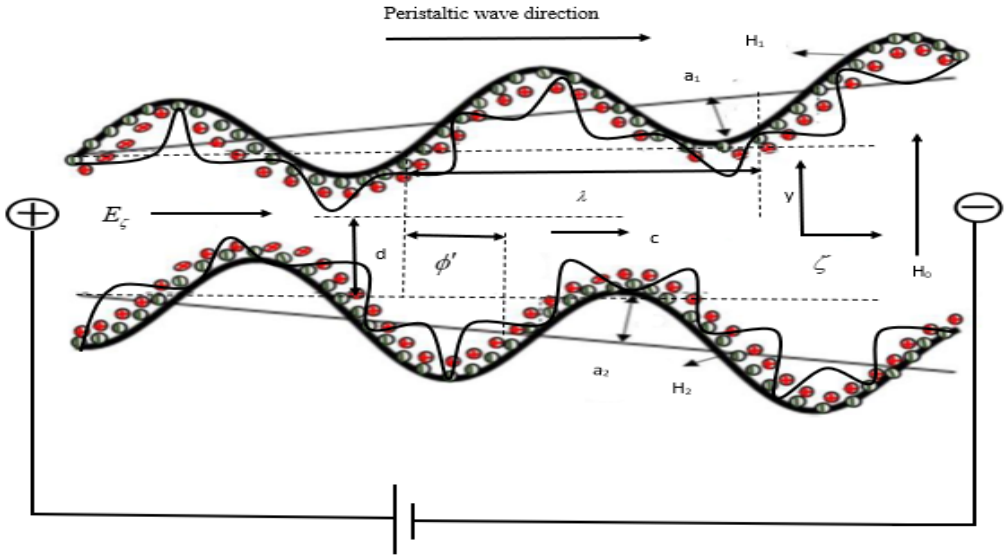

Fig. 1. Schematic diagram of a two-dimensional tapered asymmetric channel

The Eyring-Powell nanofluid is introduced into the channel. An external transverse uniform constant magnetic field of strength $\hat{H}_0$ stresses the system, which causes a magnetic field to be induced, $\hat{H}(\hat{h}_{\hat{\zeta}}(\hat{\zeta},\hat{y},\hat{t}),\hat{h}_{\hat{y}}(\hat{\zeta},\hat{y},\hat{t}),0),$ and the total magnetic field is $\hat{H}^{+}(\hat{h}_{\hat{\zeta}}(\hat{\zeta},\hat{y},\hat{t}),\hat{H}_0+\hat{h}_{\hat{y}}(\hat{\zeta},\hat{y},\hat{t}),0)$. The peristaltic wall's mathematical form is provided below :

$$H_2 = d + \hat{m}_1\hat{\zeta} + a_1 \sin\left[\frac{2\pi}{\lambda}(\hat{\zeta}-c\hat{t})\right] + b_1 \cos^4\left(\frac{\pi\hat{\zeta}}{\lambda_1}\right), \tag{1}$$

$$H_2 = -(d + \hat{m}_2\hat{\zeta} + a_2 \sin\left[\frac{2\pi}{\lambda}(\hat{\zeta}-c\hat{t})\right] + b_2 \cos^4\left(\frac{\pi\hat{\zeta}}{\lambda_2}\right)). \tag{2}$$

In above expressions $\hat{m}_1, \hat{m}_2 (<<1)$ are the non-uniform parameter of the tapered asymmetric channel, b_1 and b_2 are the height of roughness, λ_1, λ_2 are the pitch, the phase difference $\hat{\phi}$ varies in the range $0 \le \phi \le \pi$ and a_1, a_2, d and ϕ satisfies the condition,

$$a_1^2 + a_2^2 + 2a_1 a_2 d \cos\phi \le (2d)^2 . \tag{3}$$

The equations that regulate the current flow are listed below:

2.1 Fluid model

Shear stress tensor $\hat{S}$ of Eyring–Powell fluid model [33] is

$$\hat{S} = \mu \nabla \hat{V} + \frac{1}{\beta} \sinh^{-1}\left(\frac{1}{c^*} \nabla \hat{V}\right), \tag{4}$$

where μ is coefficient of shear viscosity, β and c^* are the fluid parameters

$$\sinh^{-1}\left(\frac{1}{c^*}\nabla \hat{V}\right) \approx \frac{1}{c^*} - \frac{1}{6}\left(\frac{1}{c^*}\nabla \hat{V}\right)^3, \left|\frac{1}{c^*}\nabla \hat{V}\right| \le 1 , \tag{5}$$

2.2 Maxwell's equation[29]:

$$\nabla \hat{H} = 0, \ \nabla \hat{E} = 0, \tag{6}$$

$$\nabla \wedge \hat{H} = \hat{J}, \ \hat{J} = \hat{\sigma}\{\hat{E} + \mu_e (\hat{V} \wedge \hat{H}^+)\}, \tag{7}$$

$$\nabla \wedge E = -\mu_e \frac{\partial \hat{H}}{\partial \hat{t}} , \tag{8}$$

where $\hat{E}$ induced electric field, J current density.

2.3 Induced equation is [29]:

$$\frac{\partial \hat{H}^+}{\partial \hat{t}} = \nabla \wedge \{\hat{V} \wedge \hat{H}^+\} + \frac{1}{\xi}\nabla^2 \hat{H}^+ , \tag{9}$$

where $\xi = \hat{\sigma}\mu_e$ is magnetic diffusivity.

The basic governing equations are :

$$\frac{\partial \hat{U}}{\partial \hat{\zeta}} + \frac{\partial \hat{V}}{\partial \hat{y}} = 0 , \tag{10}$$

$$\rho_f \left(\frac{\partial \hat{U}}{\partial \hat{t}} + \hat{U}\frac{\partial \hat{U}}{\partial \hat{\zeta}} + \hat{V}\frac{\partial \hat{U}}{\partial \hat{y}}\right) = -\frac{\partial \hat{p}}{\partial \hat{\zeta}} + \left(\mu_0 + \frac{1}{\beta c^{*3}}\right)\left(\frac{\partial^2 \hat{U}}{\partial \hat{\zeta}^2} + \frac{\partial^2 \hat{U}}{\partial \hat{y}^2}\right) - \frac{1}{2\beta c^{*3}}\left\{\frac{\partial \hat{U}}{\partial \hat{\zeta}} + \frac{\partial \hat{U}}{\partial \hat{y}}\right\}^2 \left(\frac{\partial^2 \hat{U}}{\partial \hat{\zeta}^2} + \frac{\partial^2 \hat{U}}{\partial \hat{y}^2}\right)$$
$$- \frac{\mu_e}{2}\left(\frac{\partial \hat{H}^{+2}}{\partial \hat{\zeta}}\right) + \mu_e\left(h_\zeta \frac{\partial h_\zeta}{\partial \hat{\zeta}} + h_\zeta \frac{\partial h_\zeta}{\partial \hat{y}} + H_0 \frac{\partial h_\zeta}{\partial \hat{y}}\right) + \rho_e E_\zeta \tag{11}$$
$$+ \rho_f g \beta_T (\hat{T} - \hat{T}_0) + \rho_f g \beta_C (\hat{\gamma} - \hat{\gamma}_0) - \left(\rho_p - \rho_{f_0}\right)\rho_f g \beta_C (\hat{\sigma} - \sigma_0),$$

$$\rho_f\left(\frac{\partial\hat{V}}{\partial\hat{t}}+\hat{U}\frac{\partial\hat{V}}{\partial\hat{\zeta}}+\hat{V}\frac{\partial\hat{V}}{\partial\hat{y}}\right)=-\frac{\partial\hat{p}}{\partial\hat{\zeta}}+\left(\mu+\frac{1}{\beta c^*}\right)\left(\frac{\partial^2\hat{V}}{\partial\hat{\zeta}^2}+\frac{\partial^2\hat{V}}{\partial\hat{y}^2}\right)-\frac{1}{2\beta c^{*3}}\left\{\frac{\partial\hat{V}}{\partial\hat{\zeta}}+\frac{\partial\hat{V}}{\partial\hat{y}}\right\}^2\left(\frac{\partial^2\hat{V}}{\partial\hat{\zeta}^2}+\frac{\partial^2\hat{V}}{\partial\hat{y}^2}\right), \quad (12)$$

$$\begin{aligned}(\rho c)_f\left(\frac{\partial\hat{T}}{\partial\hat{t}}+\hat{U}\frac{\partial\hat{T}}{\partial\hat{\zeta}}+\hat{V}\frac{\partial\hat{T}}{\partial\hat{y}}\right)&=k_T\left(\frac{\partial^2\hat{T}}{\partial\hat{\zeta}^2}+\frac{\partial^2\hat{T}}{\partial\hat{y}^2}\right)+\frac{D_{TC}\alpha C_{_P}}{C_S}\left(\frac{\partial^2\hat{\gamma}}{\partial\hat{\zeta}^2}+\frac{\partial^2\hat{\gamma}}{\partial\hat{y}^2}\right)\\&+(\rho c)_p D_B\left(\frac{\partial\hat{\sigma}}{\partial\hat{\zeta}}\frac{\partial\hat{T}}{\partial\hat{\zeta}}+\frac{\partial\hat{\sigma}}{\partial\hat{y}}\frac{\partial\hat{T}}{\partial\hat{y}}\right)+(\rho c)_p\frac{D_T}{T_m}\left[\left(\frac{\partial\hat{T}}{\partial\hat{\zeta}}\right)^2+\left(\left(\frac{\partial\hat{T}}{\partial\hat{y}}\right)^2\right)\right],\end{aligned} \quad (13)$$

$$\frac{\partial\hat{\gamma}}{\partial\hat{t}}+\hat{U}\frac{\partial\hat{\gamma}}{\partial\hat{\zeta}}+\hat{V}\frac{\partial\hat{\gamma}}{\partial\hat{y}}=D_{CT}\left(\frac{\partial^2\hat{\gamma}}{\partial\hat{\zeta}^2}+\frac{\partial^2\hat{\gamma}}{\partial\hat{y}^2}\right)+D_s\left(\frac{\partial^2\hat{T}}{\partial\hat{\zeta}^2}+\frac{\partial^2\hat{T}}{\partial\hat{y}^2}\right), \quad (14)$$

$$\frac{\partial\hat{\sigma}}{\partial\hat{t}}+\hat{U}\frac{\partial\hat{\sigma}}{\partial\hat{\zeta}}+\hat{V}\frac{\partial\hat{\sigma}}{\partial\hat{y}}=D_B\left(\frac{\partial^2\hat{\sigma}}{\partial\hat{\zeta}^2}+\frac{\partial^2\hat{\sigma}}{\partial\hat{y}^2}\right)+\frac{D_T}{T_m}\left(\frac{\partial^2\hat{T}}{\partial\hat{\zeta}^2}+\frac{\partial^2\hat{T}}{\partial\hat{y}^2}\right). \quad (15)$$

Electric potential distribution [39]:

$$\nabla^2\hat{\Phi}=-\frac{\hat{\rho}_e}{\varepsilon}, \quad (16)$$

where, $\hat{\rho}_e=ez\left(\hat{n}_1^+-\hat{n}_1^-\right)$ is the electrical charge density, $\hat{\Phi}$ is the electric potential, ε is dielectric permittivity of the medium.

Nernst-Planck equation is defined as [29]:

$$\frac{\partial\hat{n}_{1_\pm}}{\partial\hat{t}}+U\frac{\partial\hat{n}_{1_\pm}}{\partial\hat{\zeta}}+V\frac{\partial\hat{n}_{1_\pm}}{\partial\hat{y}}=D\left(\frac{\partial^2\hat{n}_{1_\pm}}{\partial\hat{\zeta}^2}+\frac{\partial^2\hat{n}_{1_\pm}}{\partial\hat{y}^2}\right)\pm\frac{Dze}{K_BT_e}\left(\frac{\partial}{\partial\hat{\zeta}}\left(\hat{n}_{1_\pm}\frac{\partial\Phi}{\partial\hat{\zeta}}\right)+\frac{\partial}{\partial y}\left(\hat{n}_{1_\pm}\frac{\partial\Phi}{\partial\hat{y}}\right)\right), \quad (17)$$

Introducing the wave frame and laboratory frame transformation in order to facilitate the analytical solutions.

$$\hat{u}=\hat{U}-c\,,\ \hat{y}=\hat{y}\,,\ \hat{v}=\hat{V}\,,\ \hat{\zeta}=\hat{\zeta}-c\hat{t}\,. \quad (18)$$

The following non dimensional variables will be introduced:

$$\left.\begin{aligned}&\psi=\frac{\hat{\psi}}{cd},\zeta=\frac{\hat{\zeta}}{\lambda},y=\frac{\hat{y}}{d},t=\frac{c\hat{t}}{\lambda},v=\frac{\hat{v}}{c},\delta=\frac{d}{\lambda},u=\frac{\hat{u}}{c},\alpha=\frac{k_T}{(\rho c)_f},\mathrm{Pr}=\frac{\mu}{\alpha},b=\frac{d}{d},m=\frac{\hat{m}\lambda}{d},\\&N_{TC}=\frac{D_{TC}\alpha C_P(\hat{\gamma}_1-\hat{\gamma}_0)}{\mu k_T C_s(\hat{T}_1-\hat{T}_0)},\theta=\frac{\hat{T}-\hat{T}_0}{\hat{T}_1-\hat{T}_0},\gamma=\frac{\hat{\gamma}-\hat{\gamma}_0}{\hat{\gamma}_1-\hat{\gamma}_0},\sigma=\frac{\hat{\sigma}-\hat{\sigma}_0}{\hat{\sigma}_1-\hat{\sigma}_0},Uhs=-\frac{E_\zeta\varepsilon\zeta}{\hat{\mu}_0c},p=\frac{{a_0}^2\hat{p}}{\lambda\mu c}\\&Nt=\frac{(\rho c)_pD_T(\hat{T}_1-\hat{T}_0)}{(\rho c)_f\mu T_m},h=\frac{\hat{h}}{d},f^*=\frac{q}{cd},Gr_t=\frac{\rho_fgd^2(\hat{T}_1-\hat{T}_0)}{c\mu},h_\zeta=\frac{\partial\phi}{\partial y},h_y=-\delta\frac{\partial\phi}{\partial\zeta},\\&\mathrm{Re}\,RmSt^2=M^2,St=\frac{H_0}{c}\sqrt{\frac{\mu_e}{\rho}},Nb=\frac{(\rho c)_pD_B(\hat{\sigma}_1-\hat{\sigma}_0)}{(\rho c)_f\mu},p_m=p+\frac{1}{2}\mathrm{Re}\,\delta\frac{\mu_e\left(\hat{H}^+\right)^2}{\rho c^2},\\&E=-\frac{E}{cH_0},K=deZ\sqrt{\frac{2n_0}{\varepsilon K_BT_e}}=\frac{d}{\lambda_d},B=\frac{1}{\mu_0\beta c^*},A=\frac{Bc^2}{2b^2c^{*2}},\Phi_1=\frac{b_1}{d},\lambda_1=\frac{\hat{\lambda}_1}{\lambda},\lambda_2=\frac{\hat{\lambda}_2}{\lambda},\\&Gr_c=\frac{\rho_fgd^2(\hat{\sigma}_1-\hat{\sigma}_0)}{c\mu},N_{CT}=\frac{D_{CT}(\hat{T}_1-\hat{T}_0)}{D_s(\hat{\gamma}_1-\hat{\gamma}_0)},Gr_F=\frac{(\rho_p-\rho_{f_0})gd^2(\hat{\gamma}_1-\hat{\gamma}_0)}{c\mu},\end{aligned}\right\} \quad (19)$$

where δ is the dimensionless wave number and the stream function is taken as $v=-\delta\frac{\partial\psi}{\partial\zeta}$ and $u=\frac{\partial\psi}{\partial y}$

The reduced non-dimensional governing equations of (11)-(15) are,

$$0=-\frac{\partial p_m}{\partial\zeta}+(1+B)\frac{\partial^3\psi}{\partial y^3}-A\left(\frac{\partial^2\psi}{\partial y^2}\right)^2\frac{\partial^3\psi}{\partial y^3}+k^2U_{HS}\Phi+\mathrm{Re}\,S_t{}^2\phi_{yy}+Gr_t\theta+Gr_c\gamma-Gr_F\sigma, \quad (20)$$

$$\frac{\partial p}{\partial y}=0, \quad (21)$$

$$(1+B)\frac{\partial^4\psi}{\partial y^4}-A\frac{\partial}{\partial y}\left\{\left(\frac{\partial^2\psi}{\partial y^2}\right)^2\frac{\partial^3\psi}{\partial y^3}\right\}+k^2U_{HS}\frac{\partial\Phi}{\partial y}-M^2\frac{\partial^2\psi}{\partial y^2}+Gr_t\frac{\partial\theta}{\partial y}+Gr_c\frac{\partial\gamma}{\partial y}-Gr_F\frac{\partial\sigma}{\partial y}=0, \quad (22)$$

$$\frac{\partial^2\theta}{\partial y^2}+N_{TC}\,\mathrm{Pr}\frac{\partial^2\gamma}{\partial y^2}+Nb\,\mathrm{Pr}\frac{\partial\theta}{\partial y}\frac{\partial\sigma}{\partial y}+Nt\,\mathrm{Pr}\left(\frac{\partial\theta}{\partial y}\right)^2=0, \quad (23)$$

$$\frac{\partial^2\gamma}{\partial y^2}+N_{CT}\frac{\partial^2\theta}{\partial y^2}=0, \quad (24)$$

$$\frac{\partial^2\sigma}{\partial y^2}+\frac{Nt}{Nb}\frac{\partial^2\theta}{\partial y^2}=0, \quad (25)$$

$$\phi_{yy}=R_m\left(E-\frac{\partial\psi}{\partial y}\right), \quad (26)$$

We get non-linear term $O\left(Pe\delta^2\right)$, after non-dimensionalization of Eq. (17). Where $Pe=Rsc$ is the ionic Peclet number and $Sc=\frac{\bar{\mu}_0}{d\rho_f}$ is Schmidt number. Using the limitations R , Pe , $\delta<<1$, the Poisson equation is obtained as:

$$\frac{\partial^2\Phi}{\partial y^2}=-k^2\left(\frac{n_{1_+}-n_{1_-}}{2}\right). \quad (27)$$

By assuming that the thickness of the EDL does not cross the channel's centreline and that the ionic distribution does not change over time, a stable Boltzmann distribution of ionic species in the EDL may be produced. As a result, the time derivative term in Eq. (17) is removed, and the dimensionless form of Eq. (17) subject to the lubrication technique is obtained,

$$0=\frac{\partial^2 n_{1_\pm}}{\partial y^2}\pm\frac{\partial}{\partial y}\left(n_{1_\pm}\frac{\partial\Phi}{\partial y}\right). \quad (28)$$

Integrating above equation with the help of boundary conditions

$$n_{1_\pm}=1\ \ \Phi=0, \quad (29)$$

$$\frac{\partial n_{1_\pm}}{\partial y}=0\ \ \frac{\partial\Phi}{\partial y}=0. \quad (30)$$

Boltzmann ionic distribution given by:
From Eq. (28) and Eq. (27) we get,

$$\frac{\partial^2\Phi}{\partial y^2}=k^2\sinh(\Phi). \quad (31)$$

Eq. (31) may be linearized using the Debye-Hückel approximation approach, which is essentially a low zeta potential assumption i.e., $\sinh\Phi \approx \Phi$, therefore Eq. (31) becomes,

$$\frac{\partial^2 \Phi}{\partial y^2} = k^2 \Phi, \tag{32}$$

now Eq. (31) can be solved directly using boundary conditions,

$$\Phi = 0 \text{ at } y = h_1, \tag{33}$$

$$\Phi = 1 \text{ at } y = h_2, \tag{34}$$

The corresponding dimensionless boundary conditions is as follows,

$$\psi = \frac{f^*}{2}, \frac{\partial \psi}{\partial y} = -1, \theta = 0, \gamma = 0, \sigma = 0 \text{ at } y = h_2 = 1 + m\zeta + a\sin[2\pi(x-t)] + \Phi_1 \cos^4\left(\frac{\pi\zeta}{\lambda_1}\right), \tag{35}$$

$$\psi = -\frac{f^*}{2}, \frac{\partial \psi}{\partial y} = -1, \theta = 1, \gamma = 1, \sigma = 1 \text{ at } y = h_1 = -1 - m\zeta - a\sin[2\pi(x-t) + \phi] - \Phi_1 \cos^4\left(\frac{\pi\zeta}{\lambda_1}\right). \tag{36}$$

Here, we have considering f^* is the mean flow over a period is,

$$\Theta' = f^* + 1, \quad f^* = \int_{h_1}^{h_2} \frac{\partial \psi}{\partial \zeta} d\zeta, \tag{37}$$

$$\text{where } \Theta' = \frac{Q}{ca_0}, \; f^* = \frac{q}{ca_0}. \tag{38}$$

The Homotopy perturbation Sumudu transformation technique (HPSTM) is used to solve the coupled partial differential equations (22)-(26) with the boundary condition (35)-(36).

3. Method of solution

Partial differential equations (22) to (26) are solved by HPSTM, to find an analytical solution, after applying the inverse Sumudu transform to (22-26), and detail about the method is given in the reference [4,38].

$$\begin{aligned} u(y) &= h_2 + y^2 a_1' + y^2 a_2' + \frac{y^3}{6(1+B)} \frac{\partial p_m}{\partial \zeta} - M^2 E \frac{y^3}{6(1+B)} \\ &+ S^{-1}\left\{\frac{\eta^3}{1+B} S\left\{\left[A\left\{\left(\frac{\partial^2 \psi}{\partial y^2}\right)^2 \frac{\partial^3 \psi}{\partial y^3}\right\} - k^2 U_{HS}\Phi + M^2\psi - Grt\theta - Grc\gamma + Grf\sigma\right]\right\}\right\}, \end{aligned} \tag{39}$$

$$\begin{aligned} \psi(y) &= h_2 f^* + y^3 a_3' + y^3 a_4' + y^3 a_5' \\ &- S^{-1}\left\{\frac{\eta^3}{1+B} S\left\{\left[\begin{array}{l} A\frac{\partial}{\partial y}\left\{\left(\frac{\partial^2 \psi}{\partial y^2}\right)^2 \frac{\partial^3 \psi}{\partial y^3}\right\} + k^2 U_{HS}\frac{\partial \Phi}{\partial y} - M^2 \frac{\partial^2 \psi}{\partial y^2} \\ + Grt\frac{\partial \theta}{\partial y} + Grc\frac{\partial \gamma}{\partial y} - Grf\frac{\partial \sigma}{\partial y} \end{array}\right]\right\}\right\}, \end{aligned} \tag{40}$$

$$\theta(y) = h_1 + y a_6' - S^{-1}\left[\eta^2 S\left\{\left[N_{TC}\,\mathrm{Pr}\frac{\partial^2 \gamma}{\partial y^2} + Nb\,\mathrm{Pr}\frac{\partial \theta}{\partial y}\frac{\partial \sigma}{\partial y} + Nt\,\mathrm{Pr}\frac{\partial^2 \theta}{\partial y^2}\right]\right\}\right], \tag{41}$$

$$\gamma(y) = h_1 + b_1' y - S^{-1}\left[\eta^2\left\{S\left[N_{CT}\frac{\partial^2\theta}{\partial y^2}\right]\right\}\right], \tag{42}$$

$$\sigma(y) = h_1 + b_2' y - S^{-1}\left[\eta^2\left\{S\left[\frac{Nt}{Nb}\frac{\partial^2\theta}{\partial y^2}\right]\right\}\right], \tag{43}$$

$$\phi(y) = b_3' y + \frac{y^2}{2}R_m E - S^{-1}\left[\eta^2\left\{S\left[R_m\frac{\partial\psi}{\partial y}\right]\right\}\right]. \tag{44}$$

Using following Eq. (45), and compare the coefficients of similar powers of P to attain the required solution,

$$H_m(U_0, U_1, U_{2,\ldots\ldots} U_m) = \frac{1}{m!}\frac{\partial^m}{\partial p^m}\left[N\left(\sum_{i=0}^{\infty} p^i U_i\right)\right]_{p=0}. \tag{45}$$

The volume flow rate is,

$$Q = \int_{h_1}^{h_2}(u+1)\,dy. \tag{46}$$

On integrating Eq. (46) we get pressure gradient and for pressure rise over one wavelength is calculated by,

$$\Delta p = \int_0^1 \frac{\partial p}{\partial \zeta} d\zeta\,. \tag{47}$$

Use following equation to calculate the axial induced magnetic field [25],

$$h_\zeta = -\frac{\partial \phi}{\partial y}. \tag{48}$$

4. Discussion

The Mathematica software is employed to obtain the numerical results for equations (39 to 48). We have compared the acquired results with numerical results of Praksha *et al.,* [21] as shown in table 1. It is determined to be in good accord with the findings of the current investigation.

Table 1
Comparison between present analytical solution with Prakash *et al.,* [21],solution for different values of y when $Q=2$, $Gr_C=0$, $Gr_F=0$, $Gr_t=0$, $U_{HS}=0$, $k=0$, $\Phi_1=0$, $A=0$, $B=0$

y	Prakash *et al.,*[21]	Present work
1.0	2	2
0.8	2.032	2.03328
0.6	1.776	1.7732
0.4	1.304	1.30624
0.2	0.688	0.684
0.5	1.5625	1.5625
0.0	0	0

4.1 Flow distribution

Figures 2(a) to 2(i) represents the influence of nanoparticle Grashoff number Gr_F, solutal Grashoff number Gr_C, thermal Grashoff number Gr_t, Helmholtz-Smoluchowski velocity U_{HS}, electroosmotic parameter k on velocity u. Eyring-Powell fluid parameter A and B, Hartman number M, rough surface Φ_1 with varying fluid parameter $B=1,1.2,1.4$ respectively on velocity profile. Figure 2(a) portrait the effect of Gr_f on flow parameter u. It is noted that as Grf increases, u drops. It is because Grashoff number is inversely proportional to the viscosity of fluid particles resulting in a decrease in u. Opposite behaviour can be seen in both Gr_C and Gr_t from figure 2(b) and figure 2(c) it is noted that is maximum velocity attains for values of Gr_C, whereas minimum velocity occurs for the values of Grt because both Grashoff numbers satisfies the relative influence of viscous hydrodynamic force and thermal buoyancy force. The effect of $U_{HS}=-1,0,1$ on u is observed in figure 2(d), where the velocity for purely peristaltically driven flow is shown by the curve $U_{HS}=0$. Also, it's worth noting that the velocity increases as the amplitude of the electric field increases, implying that electroosmosis can improve peristaltic flow. Impact of EDL (Debye) thickness on u can be seen in figure 2(e). With rising electroosmotic parameter k, there is a substantial acceleration in axial velocity in the channel. Here, k is the ratio of Debye thickness to channel width. An increase in Debye length induces a drop in the EDL, implying that bulk fluid motion occurs quickly. From figure 2(f) and figure 2(g) one can observe that u decreases as Eyring -Powell fluid parameter increases. It is obvious that fluid parameters are inversely proportional to the viscosity of the fluid. Velocity u decreases when M is enhanced. For fluid flow, the Lorentz force serves as a retarding force. As a result, the fluid flow gets slow down by the magnetic force, which is shown in figure 2(h). Such studies have uses in medicine, such as regulating blood flow and preventing blood clotting. Figure 2(i) shows that as roughness parameter Φ_1 increases u decreases. It is due to an increase in the contact area of the fluid to the surface roughness and also because of boundary effects, a surface roughness across an arbitrary amount drastically reduces the apparent viscosity of blood.

4.2 Pressure gradient

Figures 3(a)-3(f) represents the impact of solute lGrashoff number Gr_C, nanoparticle Grashoff number Gr_f, thermal Grashoff number Gr_t, Helmholtz-Smoluchowski velocity U_{HS}, electroosmotic parameter k, roughness parameter Φ_1 respectively on pressure ΔP. Figure 3(a) and figure 3(b) indicates the ΔP for different values of Gr_C and Gr_f.It is noticed that the maximum pressure is attains for higher values of Gr_C and Gr_f. Since the concentration of nanoparticles in the fluid increases, resulting in a decrease in pressure. Figure 3(c) shows the ΔP for different values Gr_t that is the ΔP increases with an increase in Gr_t. The influence of $U_{HS}=-\frac{E_\varsigma \varepsilon \zeta}{\bar{\mu}_0 c}$ on peristalsis is relevant to analyse as pumping mechanism of peristaltic is shown in figure 3(d). U_{HS} depends on the external electric field. $U_{HS}=0,1,2$ are considered to analyse the peristalsis characteristics, i.e., without electric field ($U_{HS}=0$) and with opposing the electric field ($U_{HS}=1,2$). We can see that as U_{HS} increases ΔP also increases. The effect of EDL thickness on pumping characteristics can be seen in figure 3(e) We can observe that the ΔP decreases by increasing the magnitude of k .That is, if EDL thickness is greater, more pressure is necessary to drive the ionic nano-liquids (i.e., less magnitude of electroosmotic parameter). The formation of an EDL on a charged surface is physically understood as a barrier to the flow of ionic

liquids. From figure 3(f) we can observe that as roughness parameter increases ΔP also increases. It is due to an increase in Φ_1, the cross-sectional area decreases. As a result, channels with a rougher surface have lower flow area, so ΔP increases.

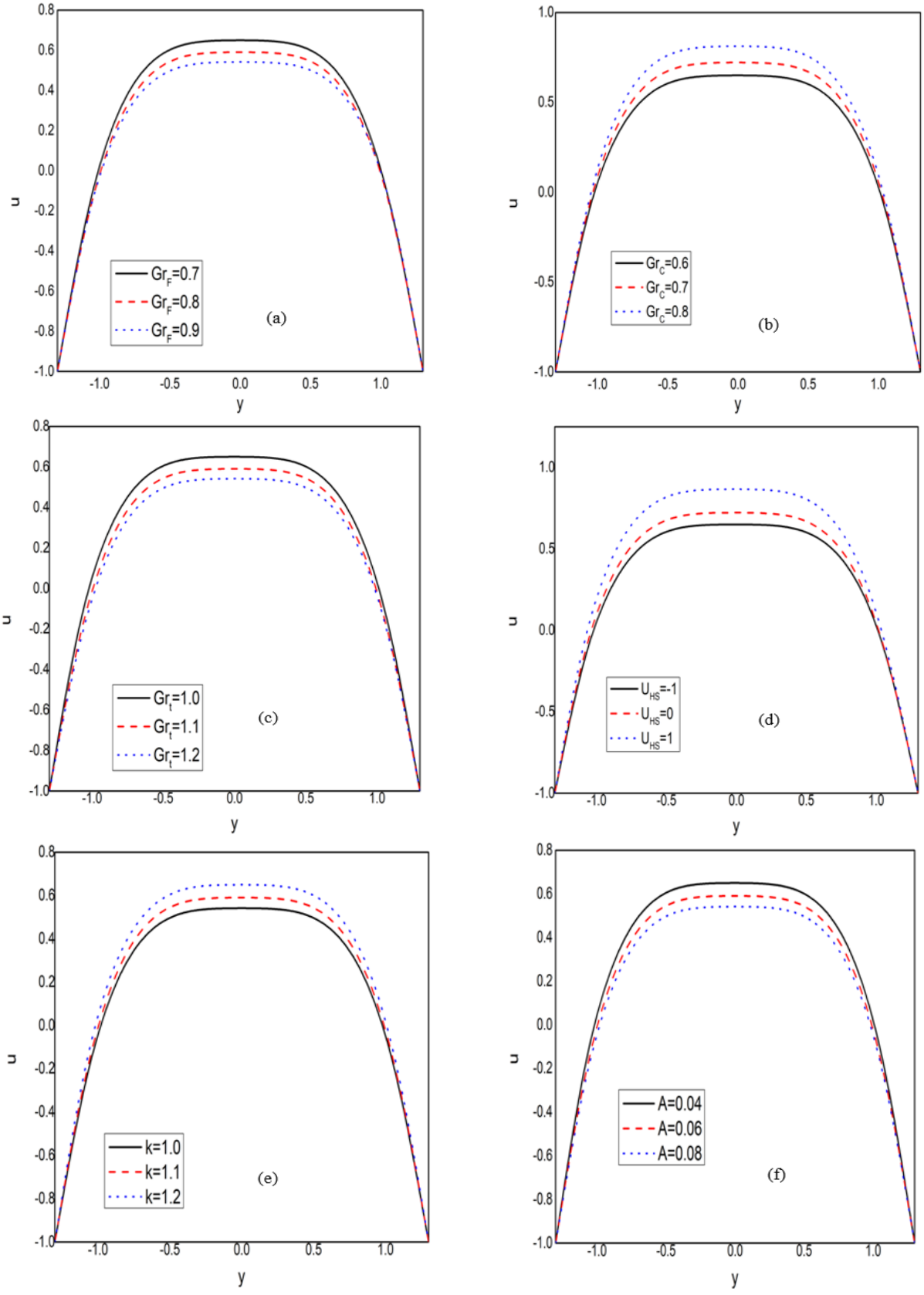

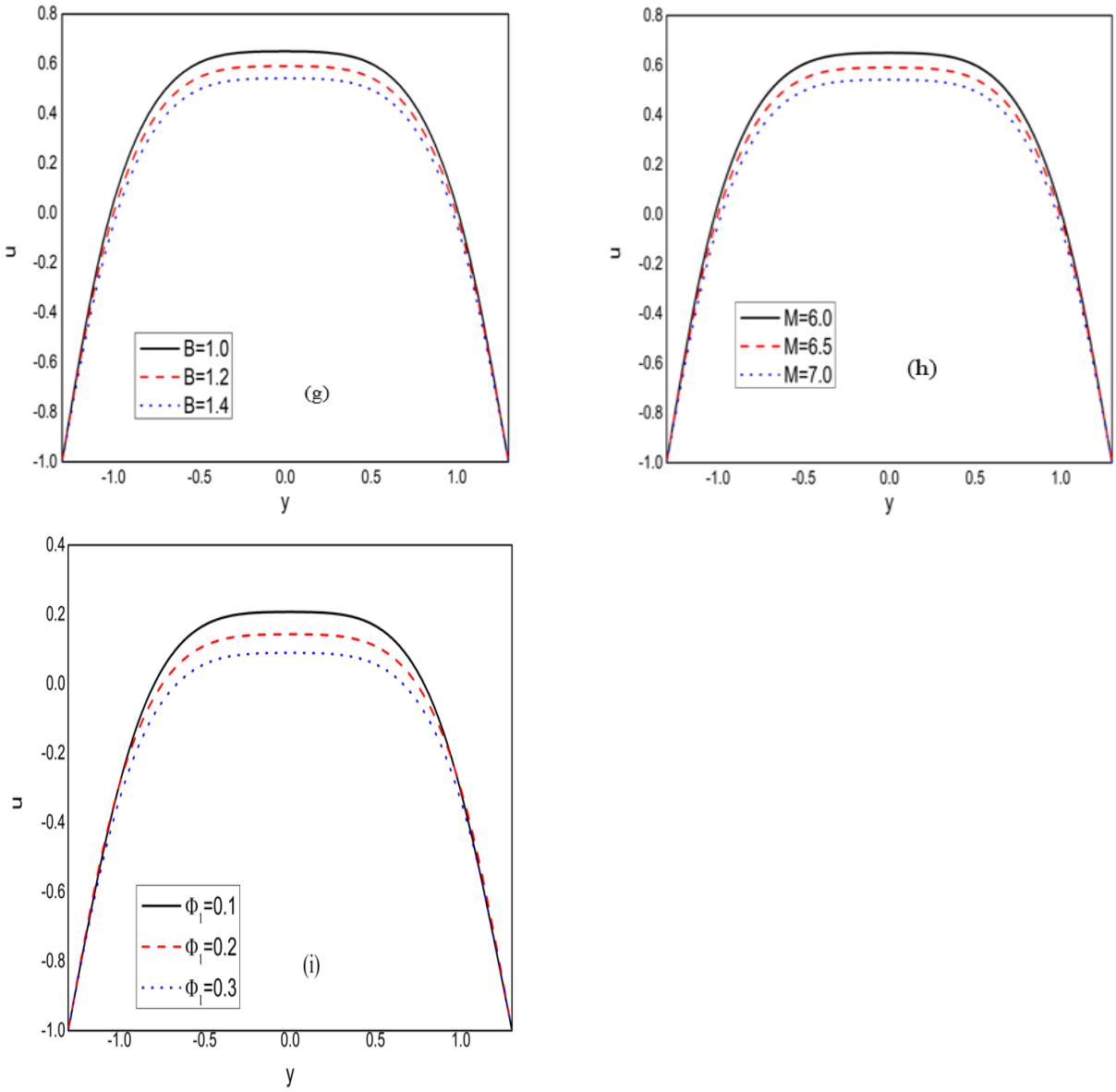

Fig. 2: Velocity profile (a) Gr_F when $A=0.04, k=1, Gr_t=1, Gr_C=0.6,\ M=7, U_{HS}=-1$ (b) Gr_C when $A=0.04, k=1, Gr_t=1, Gr_F=0.6, M=7, U_{HS}=-1$ (c) Gr_t when $A=0.04, k=1, Gr_C=0.6,\ Gr_F=0.6, M=7, U_{HS}=-1$ (d) U_{HS} when $A=0.04, k=1, Gr_t=1, Gr_C=0.6, Gr_F=0.6, M=7$ (e) k when $A=0.04, Grt=1, Grc=0.6, Grf=0.6, M=7, U_{HS}=-1$ (f) A for $k=1, Grt=1, Grc=0.6, Grf=0.6, M=7,$ (g) B when $k=1, Grt=1, Grc=0.6, Grf=0.6, M=7,$ (h) Magnetic field M when $A=0.04, k=1, Gr_t=1, Gr_C=0.6, Gr_F=0.6$ (i) ϕ_1 when $k=1, Grt=1, Grc=0.6, Grf=0.6, M=7,$

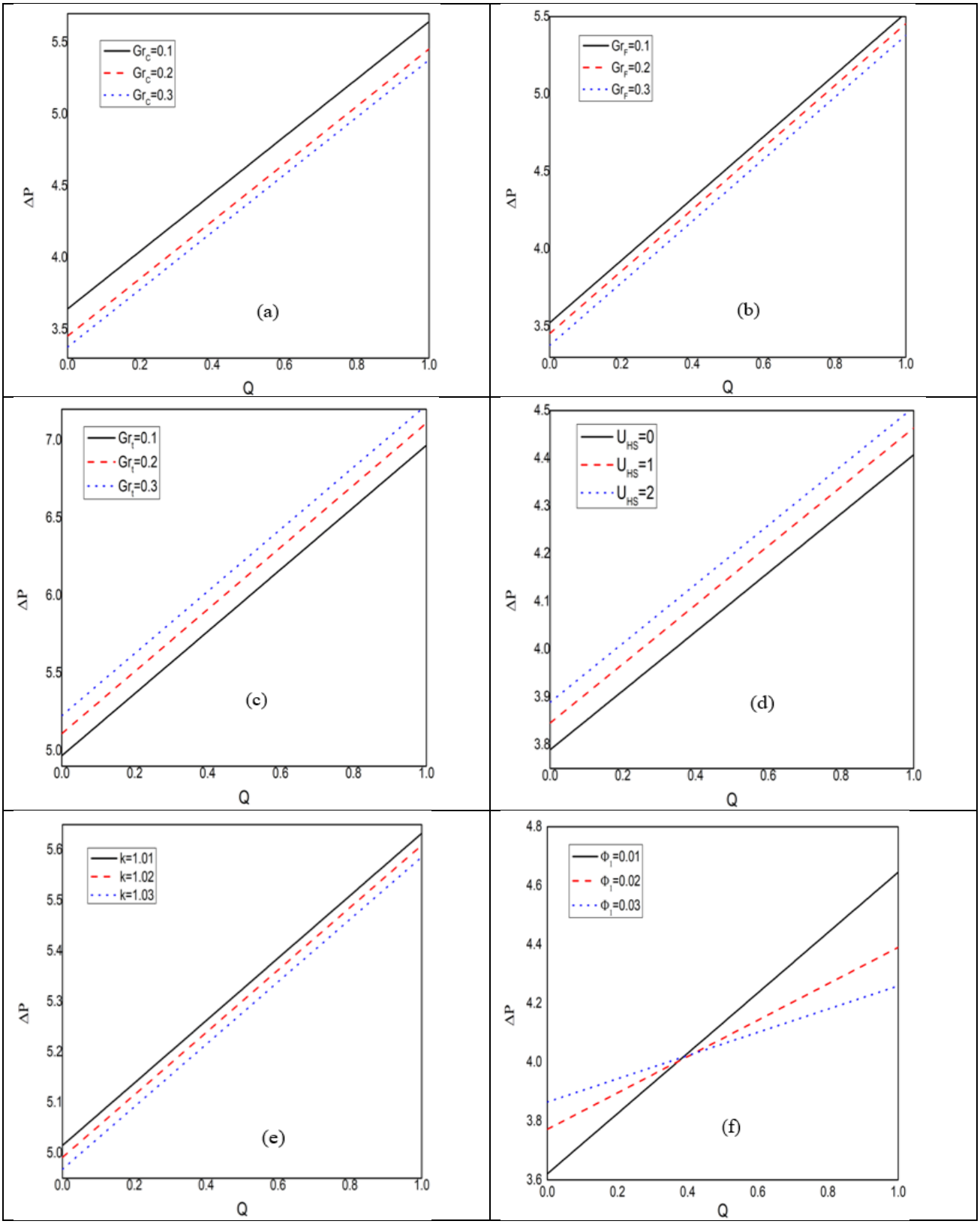

Fig. 3. Pressure rise for different values of (a) Gr_C for $A=0.1, B=1, k=0.1, Gr_t=1, Gr_F=1,$ (b) Gr_F for $A=0.1, B=1, k=0.1, Gr_t=1, Gr_C=1, M=1.2, U_{HS}=1$ (c) Gr_t for $A=0.1, B=1,$ $k=0.1, Gr_C=1, Gr_F=1, M=1.2, U_{HS}=1$ (d) U_{HS} when $A=0.1, B=1, k=0.1, Gr_t=1, Gr_C=1, Gr_F=1, M=1.2$ (e) k for $A=0.1, B=1, Gr_C=1, Gr_F=1, Gr_t=1, M=1.2, U_{HS}=1$ (f) Φ_1 for $A=0.1, B=1, k=0.1, Gr_t=1, Gr_C=1, Gr_F=1, M=1.2, U_{HS}=1$

4.3 Temperature profile, Solutal (species) concentration profile and Nanoparticle volume fraction distribution

Figures 4(a) and 4(b) illustrates the causes of Brownian motion parameter Nb amd thermophoresis parameter Nt on temperature θ. It is observed that there is improvement in θ for changed values of Nb and Nt. The scattering of fluid particles enables more heat to be created as Nb in the system grows larger, causing temperature rises, shown in figure 4(a). Whereas, in figure 4(b), the θ attains maximum temperature by raising Nt, because fluid particles are move towards heated region from the cold surface region. The variation of Nt and Nb for concentration profile γ are portrayed in figure 5(a) and 5(b) respectively. From these two figures, one can observe that the γ has the similar behaviour on both Nt and Nb, due to rise in temperature the concentration of particles decays in system hence for enhancing the values of Nt and Nb the concentration γ decreases. Figures 6(a) and 6(b) are plotted to show the Nb and Nt effects on volume fraction σ. Opposite behaviour can be seen in case of Nb and Nt for σ because the heat distribution of nanofluids is large in system, therefore Nt increases cause the nanoparticle volume fraction declines, whereas in case of the Nb opposite can be observed.

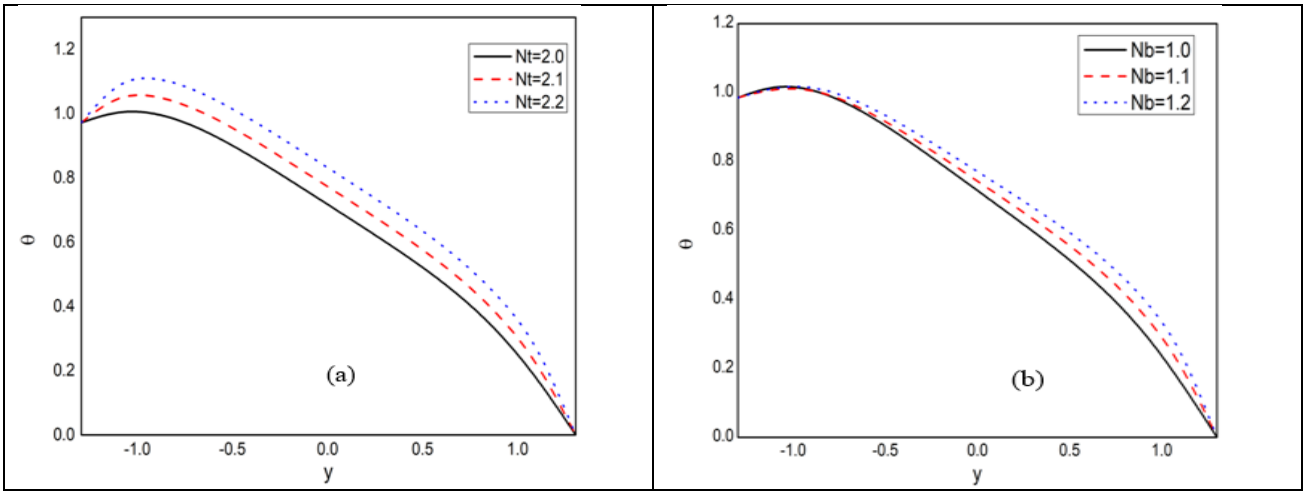

Fig. 4. Temperature profile for (a) Nt when $Nb = 0.6, N_{TC} = 0.5, N_{CT} = 0.5, \Pr = 7$ (b) Nb when $Nt = 0.6, N_{TC} = 0.5, N_{CT} = 0.5, \Pr = 7$

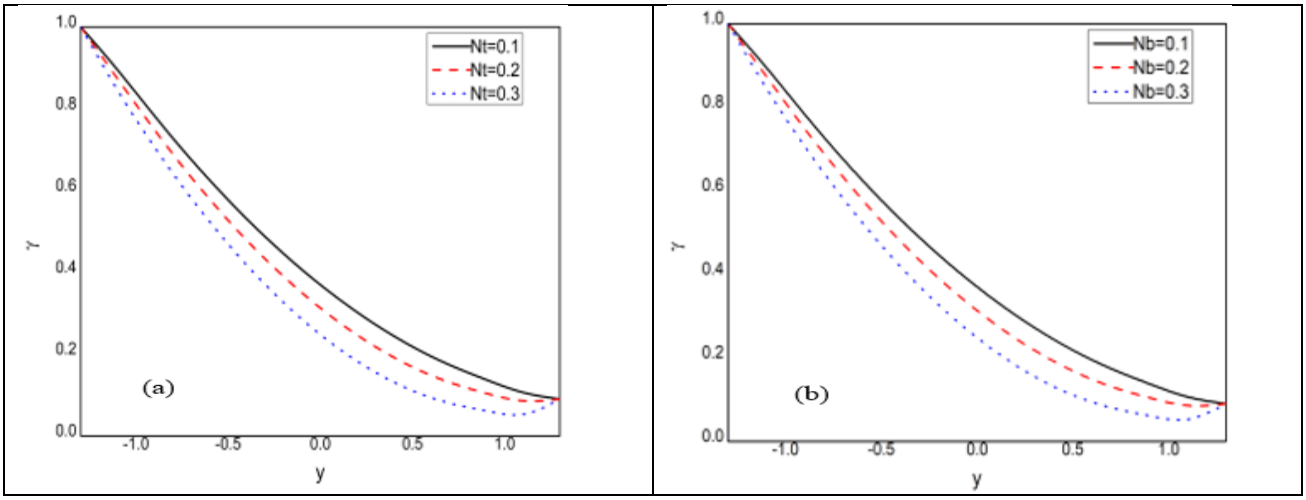

Fig. 5. Concentration profile for various values of (a) Nt for $Nb = 0.6, N_{TC} = 0.5, \Pr = 7$ (b) Nb for $Nt = 0.6, N_{TC} = 0.5, \Pr = 7$

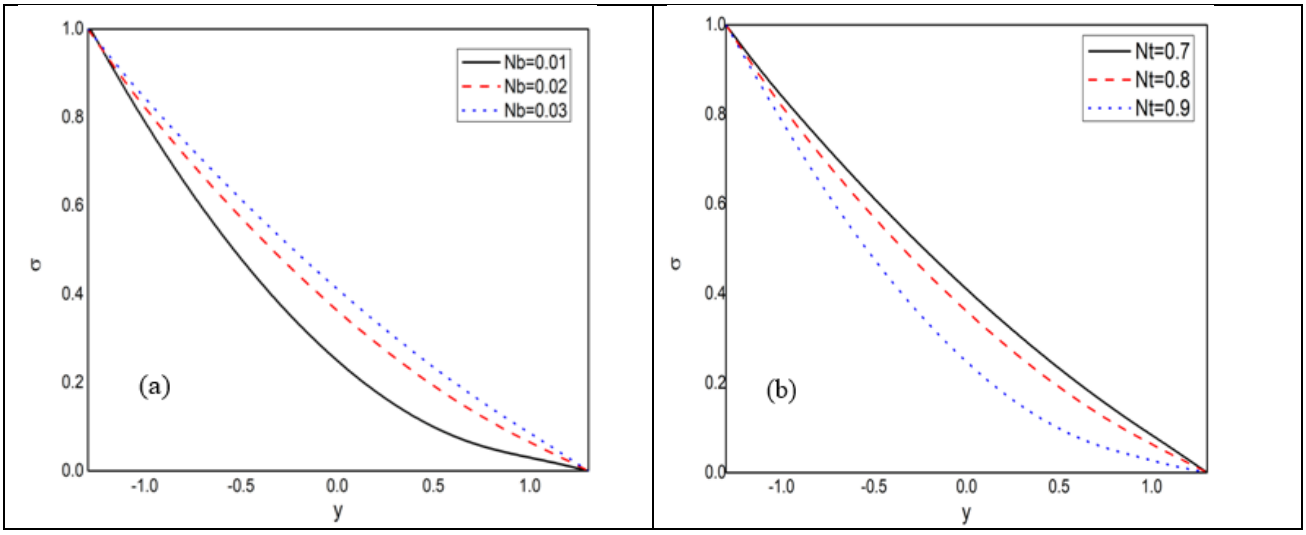

Fig. 6. Volume fraction profile for (a) Nb when $Nt = 0.6, N_{TC} = 0.5, \Pr = 7$ (b) Nt when $Nb = 0.6, N_{TC} = 0.5, \Pr = 7$

Magnetic field characteristics and Magnetic force function

Axial induced magnetic field h_ζ against y for various rates of induced electric field E and magnetic Reynolds number R_m are shown in figures 7(a) and 7(b) respectively. It is noted that h_ζ declines as values of R_m and E attains maximum values in the region $-0.3 \le y \le 0$, opposite action take place in the region $0 \le y \le 0.3$. The expressions for magnetic force function ϕ against y for different values of R_m and E are shown in figure 8(a) and figure 8(b). Similar behaviour is observed, that is with the increase in R_m and E, ϕ decreases.

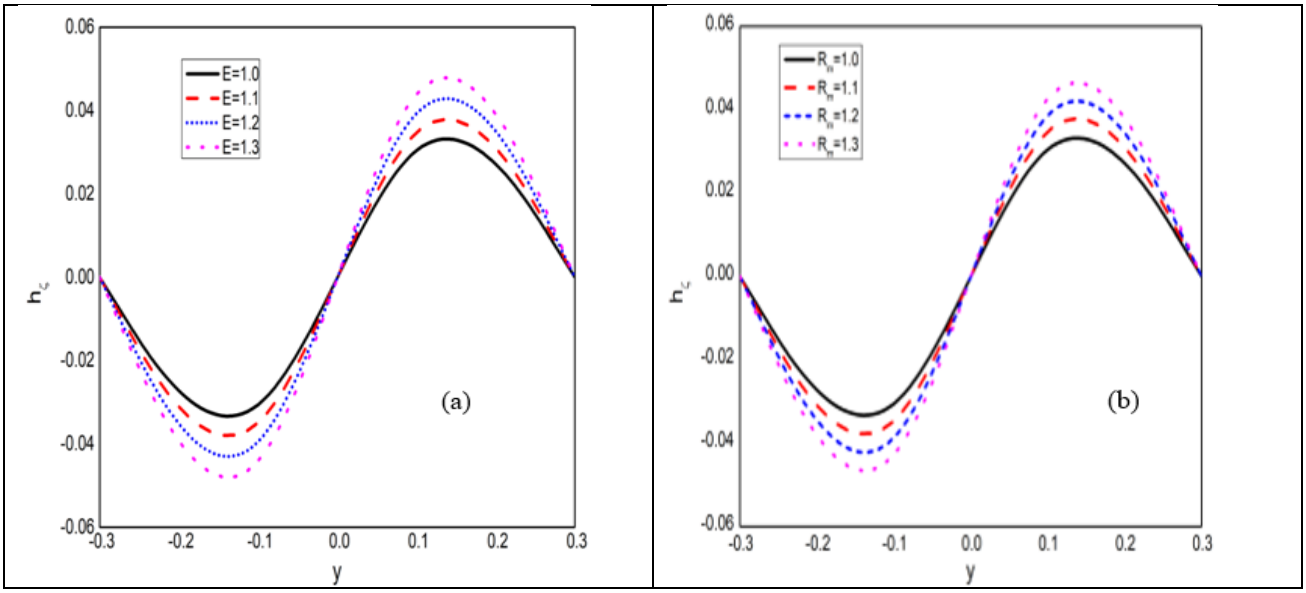

Fig. 7. Axial induced magnetic field for (a) $_E$ when $A = 0.7, B = 4, R_m = 1$ (b) R_m when $A = 0.7, B = 4, E = 1$

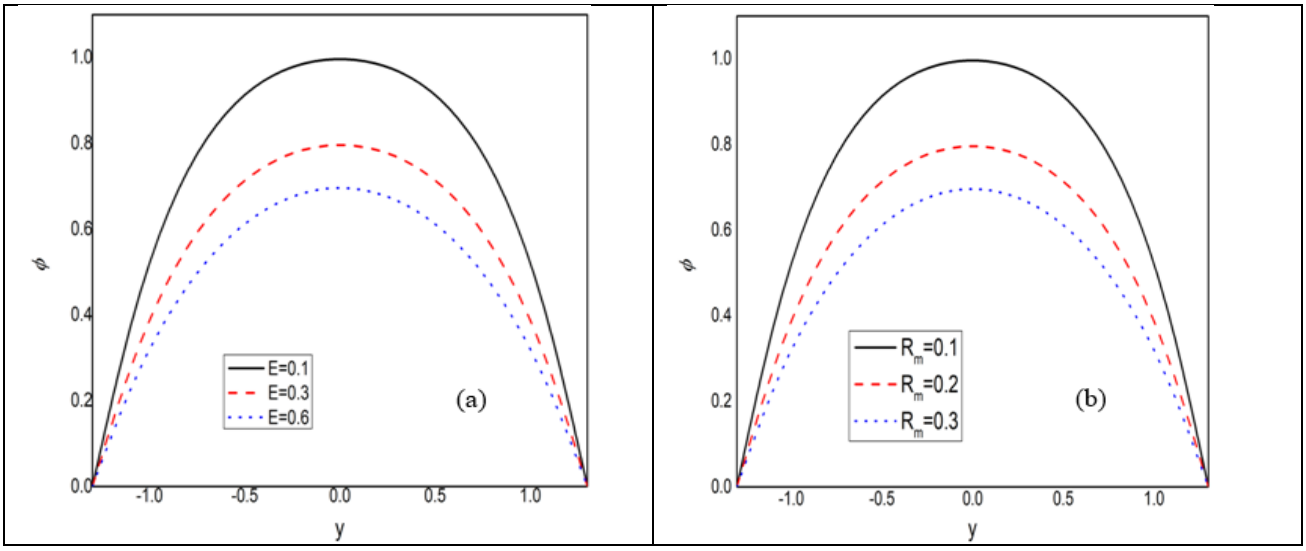

Fig. 8. Magnetic force function for various values (a) $_E$ for $A=0.7, B=1, R_m=0.1$ (b) R_m for $A=0.7, B=4, E=0.1$

4.4 Trapping Phenomena

Figures 9(a) and 9(b) illustrate the effect of induced electric field E, one can observe that with rising values of E, bolus decreases in size. Figures 10(a) to 10(c) shows the effect of M on streamlines. We can observe that the bolus decreases in size as M increases. Roughness parameter Φ_1 on streamlines can be observed in figures 11(a) to 11(c). Here as we increase the roughness parameter outer surface of the bolus becomes rough.

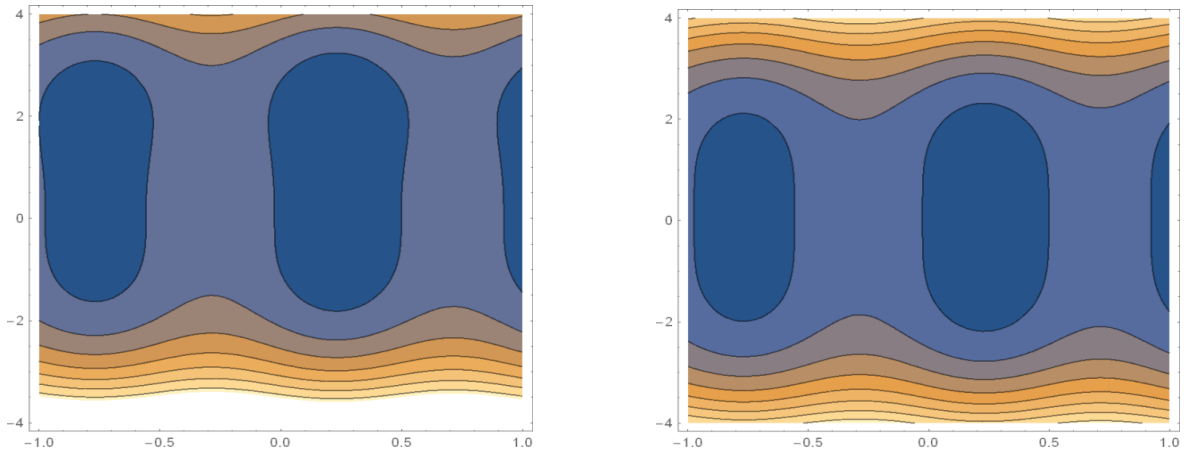

(a) (b)

Fig. 9. Plots of streamlines when (a) $E=0.4$ (b) $E=1.0$ for $A=0.3, B=1, Q=2, Grc=1, Grf=0.6, Grt=1, M=1, U_{HS}=-1, \Phi_1=0.01$

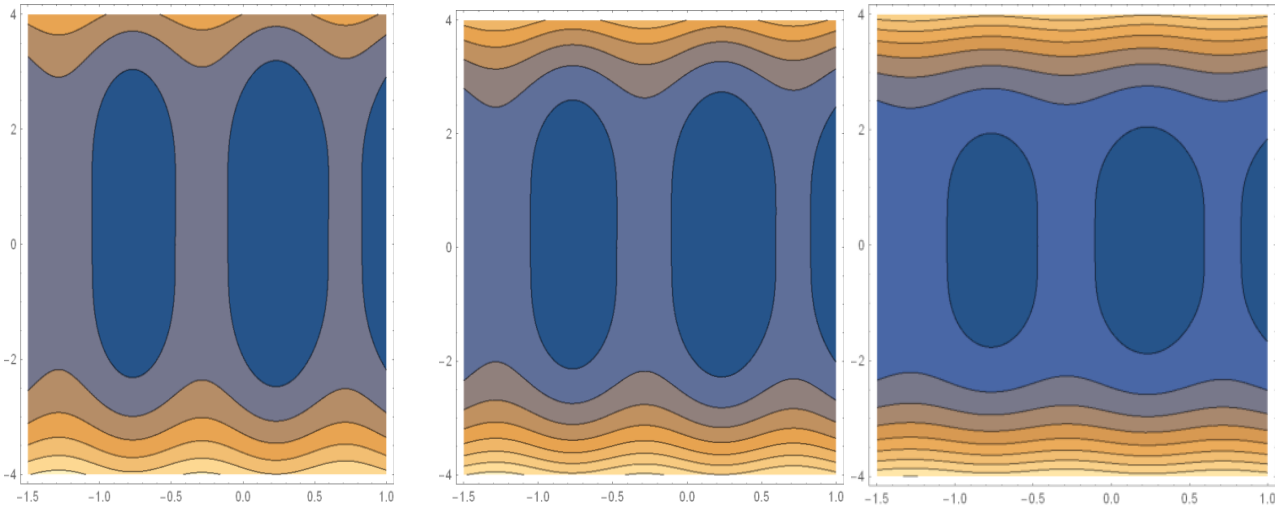

(a) (b) (c)

Fig. 10. Plots of streamlines when (a) M =0.8, (b) M =1, (c) M =1.6 for $A=0.3, B=1, Q=2,$ $E=1, Gr_C=1, Gr_F=0.6, Gr_t=1, U_{HS}=-1, \Phi_1=0.01$.

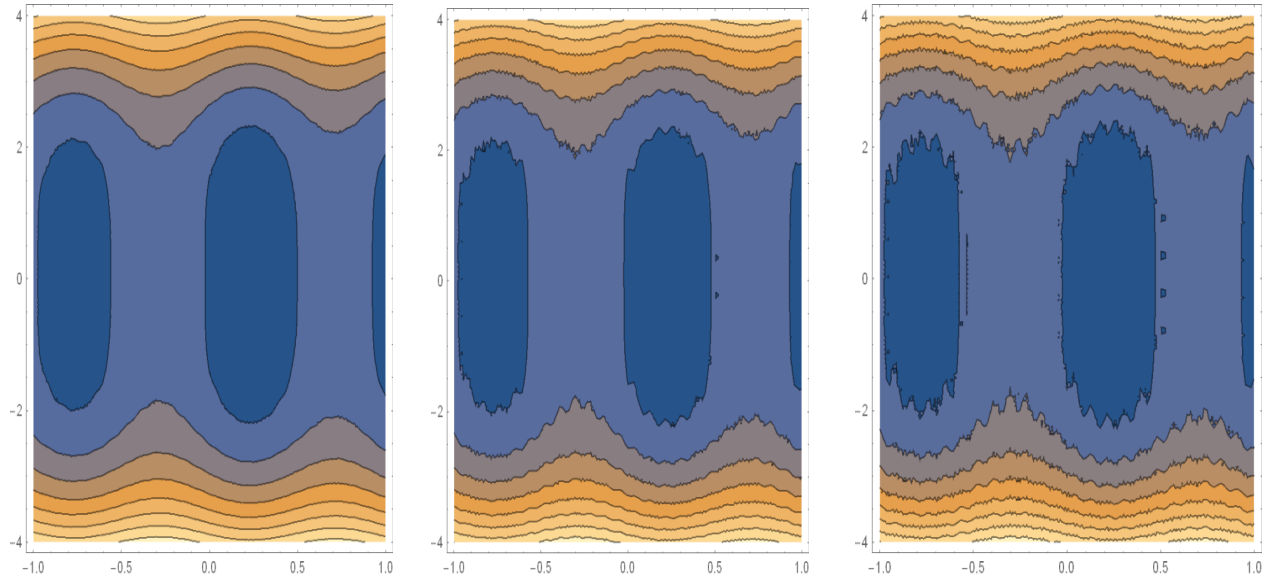

(a) (b) (c)

Fig. 11. Plots of streamlines when (a) Φ_1 =0.01, (b) Φ_1 =0.04, (c) Φ_1 =0.07 for $A=0.3, B=1, Q=2, E=1, Gr_C=1, Gr_F=0.6, Gr_t=1, U_{HS}=-1, M=1$.

5. Conclusions

In this article, we have studied the effect of induced magnetic field with electro-osmosis peristaltic flow with double diffusion of Eyring Powell nanofluid in a tapered asymmetric channel having sinusoidal roughness. The dimensionless nonlinear equations are solved by the by STM with the help of homotopy perturbation method. Present study is in good agreement with previous study [21]. Present study is useful in the study of surface roughness of biological organs, such as blood flow in coronary arteries, and all other surfaces have roughness up to some extent. Surface roughness can be used to identify diseases within biological tissues. The main observations are summarized below,

- Behaviour of Gr_F and Gr_t is similar on velocity profile.

- Similar behaviour can be monitored on velocity profile on varying U_{HS}, k.
- A, B are Eyring-Powell fluid parameter behaving similar on velocity profile .
- Velocity profile decreases as M and Φ_1 increases.
- Behaviour of Gr_F and Gr_C is similar on pressure rise.
- Opposite behaviour can be observed on pressure rise on varying U_{HS}, k.
- It is worth noticing that as Φ_1 increases pressure rise also increases.
- Nb and Nt behaves similar on temperature profile and concentration profile. That is both Nb and Nt increases on temperature profile and decreases on concentration profile, also opposite behaviour can be seen on volume fraction as Nb and Nt increases.
- R_m and E behaves similar in the region $-0.3 \le y \le 0$, i.e., h_ζ decreases and while in the region $0 \le y \le 0.3$, h_ζ increases.
- Important finding of this study is as roughness parameter increases surface of the bolus becomes rough.

References

[1] Latham T.W. Fluid motion in peristaltic pump: M.S. Thesis MI. Cambridge: MA;1966.
[2] Shapiro, Ascher H., Michel Yves Jaffrin, and Steven Louis Weinberg. "Peristaltic pumping with long wavelengths at low Reynolds number." *Journal of Fluid Mechanics* 37, no. 4 (1969): 799-825.
[3] Jaffrin, M. Y., and A. H. Shapiro. "Peristaltic pumping." *Annual review of fluid mechanics* 3 (1971): 13-37.
[4] Asha S. K., and Namrata K. "Thermal analysis for Peristaltic flow of nanofluid under the influence of porous medium and double diffusion in non-uniform channel using Sumudu Transformation Method." Annul of pure and applied Mathematics 2021; 23(2):73-91.
[5] Asha S K, Sunitha, G. "Influence of thermal radiation on peristaltic blood flow of a Jeffrey fluid with double diffusion in the presence of gold nanoparticles." *Informatics in Medicine Unlocked* 17 (2019): 100272.
[6] Ali, Aamir, Y. Ali, D. N. Khan Marwat, M. Awais, and Z. Shah. "Peristaltic flow of nanofluid in a deformable channel with double diffusion." *SN Applied Sciences* 2, no. 1 (2020): 1-10.
[7] Burton, Hanna E., and Daniel M. Espino. "The effect of mechanical overloading on surface roughness of the coronary arteries." *Applied bionics and biomechanics* 2019 (2019).
[8] Park, Sang Woo, Marcos Intaglietta, and Daniel M. Tartakovsky. "Impact of endothelium roughness on blood flow." *Journal of theoretical biology* 300 (2012): 152-160.
[9] Darcy, N. "Recherches experimentales relatives au mouvement de l'eau dans des tuyaux." *Mem. savants etrangers Acad. Sci. Inst. Fr.* 15 (1858): 141.
[10] Han, J. C., Y. M. Zhang, and C. P. Lee. "Augmented heat transfer in square channels with parallel, crossed, and V-shaped angled ribs." (1991): 590-596.
[11] Taylor, James B., Andres L. Carrano, and Satish G. Kandlikar. "Characterization of the effect of surface roughness and texture on fluid flow—past, present, and future." *International journal of thermal sciences* 45, no. 10 (2006): 962-968.
[12] Wagner, Rebecca N., and Satish G. Kandlikar. "Effects of structured roughness on fluid flow at the microscale level." *Heat transfer engineering* 33, no. 6 (2012): 483-493.
[13] Dharaiya, V. V., and S. G. Kandlikar. "A numerical study on the effects of 2d structured sinusoidal elements on fluid flow and heat transfer at microscale." *International journal of heat and mass transfer* 57, no. 1 (2013): 190-201.
[14] Shukla, R., A. Medhavi, S. S. Bhatt, and R. Kumar. "Mathematical analysis of heat transfer in peristaltic transport through a rough nonuniform inclined channel." *Mathematical Problems in Engineering* 2020 (2020).
[15] Shukla, R., S. S. Bhatt, A. Medhavi, and R. Kumar. "Effect of Surface Roughness during Peristaltic Movement in a Nonuniform Channel." *Mathematical Problems in Engineering* 2020 (2020).
[16] Eytan, Osnat, Ariel J. Jaffa, and David Elad. "Peristaltic flow in a tapered channel: application to embryo transport within the uterine cavity." *Medical engineering & physics* 23, no. 7 (2001): 475-484.
[17] Kothandapani, M., and J. Prakash. "Effects of thermal radiation parameter and magnetic field on the peristaltic motion of Williamson nanofluids in a tapered asymmetric channel." *International Journal of Heat and Mass Transfer* 81 (2015): 234-245.

[18] Hayat, T., Rija Iqbal, Anum Tanveer, and Ahmed Alsaedi. "Influence of convective conditions in radiative peristaltic flow of pseudoplastic nanofluid in a tapered asymmetric channel." *Journal of Magnetism and Magnetic Materials* 408 (2016): 168-176.

[19] Eldabe, Nabil T., Galal M. Moatimid, Abdelhafeez A. ElShekhipy, and Naglaa F. Aballah. "Mixed convective peristaltic flow of Eyring-Prandtl fluid with chemical reaction and variable electrical conductivity in a tapered asymmetric channel." *Heat Transfer—Asian Research* 48, no. 5 (2019): 1946-1962.

[20] Tanveer, Anum, Sidra Mahmood, Tasawar Hayat, and Ahmed Alsaedi. "On electroosmosis in peristaltic activity of MHD non-Newtonian fluid." *Alexandria Engineering Journal* 60, no. 3 (2021): 3369-3377.

[21] Jayavel, Prakash, Ravinder Jhorar, Dharmendra Tripathi, and Martin N. Azese. "Electroosmotic flow of pseudoplastic nanoliquids via peristaltic pumping." *Journal of the Brazilian Society of Mechanical Sciences and Engineering* 41, no. 2 (2019): 1-18.

[22] Chaube, Mithilesh Kumar, Ashu Yadav, Dharmendra Tripathi, and O. Anwar Bég. "Electroosmotic flow of biorheological micropolar fluids through microfluidic channels." *Korea-Australia Rheology Journal* 30, no. 2 (2018): 89-98.

[23] Tanveer, Anum, Sidra Mahmood, Tasawar Hayat, and Ahmed Alsaedi. "On electroosmosis in peristaltic activity of MHD non-Newtonian fluid." *Alexandria Engineering Journal* 60, no. 3 (2021): 3369-3377.

[24] Hayat, T., and N. Ali. "Peristaltically induced motion of a MHD third grade fluid in a deformable tube." *Physica A: Statistical Mechanics and its applications* 370, no. 2 (2006): 225-239.

[25] Akram, Safia, and S. Nadeem. "Influence of induced magnetic field and heat transfer on the peristaltic motion of a Jeffrey fluid in an asymmetric channel: closed form solutions." *Journal of Magnetism and Magnetic Materials* 328 (2013): 11-20.

[26] Mekheimer, Kh S. "Effect of the induced magnetic field on peristaltic flow of a couple stress fluid." *Physics Letters A* 372, no. 23 (2008): 4271-4278.

[27] Vishnyakov, V. I., and K. B. Pavlov. "Peristaltic flow of a conductive liquid in a transverse magnetic field." *Magnetohydrodynamics* 8, no. 2 (1972): 174-178.

[28] Akram, Safia, and Qamar Afzal. "Effects of thermal and concentration convection and induced magnetic field on peristaltic flow of Williamson nanofluid in inclined uniform channel." *The European Physical Journal Plus* 135, no. 10 (2020): 1-28.

[29] Rashid, M., K. Ansar, and S. Nadeem. "Effects of induced magnetic field for peristaltic flow of Williamson fluid in a curved channel." *Physica A: Statistical Mechanics and its Applications* 553 (2020): 123979.

[30] Javid, Khurram, Mohsan Hassan, Dharmendra Tripathi, Salahuddin Khan, Elena Bobescu, and Muhammad Mubashir Bhatti. "Double-diffusion convective biomimetic flow of nanofluid in a complex divergent porous wavy medium under magnetic effects." *Journal of Biological Physics* 47, no. 4 (2021): 477-498.

[31] Shivappa Kotnurkar, Asha, and Sunitha Giddaiah. "Double diffusion on peristaltic flow of nanofluid under the influences of magnetic field, porous medium, and thermal radiation." *Engineering Reports* 2, no. 2 (2020): e12111.

[32] Asha, S. K., and G. Sunitha. "Mixed convection peristaltic flow of a Eyring–Powell nanofluid with magnetic field in a non-uniform channel." *JAMS* 2, no. 8 (2018): 332-334.

[33] Asha, S. K., and G. Sunitha. "Peristaltic transport of Eyring-Powell nanofluid in a non-uniform channel." *Jordan J Math Stat* 12, no. 3 (2019): 431-453.

[34] Weerakoon, Sunethra. "Application of Sumudu transform to partial differential equations." *International Journal of Mathematical Education in Science and Technology* 25, no. 2 (1994): 277-283.

[35] Belgacem, Fethi Bin Muhammed, Ahmed Abdullatif Karaballi, and Shyam L. Kalla. "Analytical investigations of the Sumudu transform and applications to integral production equations." *Mathematical problems in Engineering* 2003, no. 3 (2003): 103-118.

[36] Watugala, GK1206847. "Sumudu transform: a new integral transform to solve differential equations and control engineering problems." *Integrated Education* 24, no. 1 (1993): 35-43.

[37] Watugala, GK1206847. "Sumudu transform: a new integral transform to solve differential equations and control engineering problems." *Integrated Education* 24, no. 1 (1993): 35-43.

[38] Eltayeb, Hassan, and Adem Kilicman. "A note on the Sumudu transforms and differential equations." *Applied Mathematical Sciences* 4, no. 22 (2010): 1089-1098.